Single-cell RNA-sequencing analysis reveals the molecular mechanism of subchondral bone cell heterogeneity in the development of osteoarthritis

Yan Hu[1], Jin Cui[2], Han Liu[1], Sicheng Wang[3], Qirong Zhou[2], Hao Zhang[2], Jiawei Guo[2], Liehu Cao[4*], Xiao Chen[2*], Ke Xu[1*], Jiacan Su[1,2*]

[1] Institute of Translational Medicine, Shanghai University, Shanghai 200444, China.

[2] Department of Orthopedics, Shanghai Changhai Hospital, Naval Medical University, Shanghai 200433, China.

[3] Department of Orthopedics, Shanghai Zhongye Hospital, Shanghai 200941, China.

[4] Department of Orthopedics, Shanghai Baoshan Luodian Hospital, Shanghai 201908, China.

YH, XC, JC and SW contributed equally.

Correspondence should be addressed to traumahu@163.com (L.H.C.); sirchenxiao@126.com (X.C.); kexu@shu.edu.cn (K.X.); drsujiacan@163.com (J.C.S.)

Short title: Cell heterogeneity in OA subchondral bone

Abstract

The cellular composition and underlying spatiotemporal transformation processes of subchondral bone in osteoarthritis (OA) remain unknown. Herein, various cell subsets from tibial plateau of OA patients are identified, and the mechanism of subchondral microstructure alteration is elaborated using single-cell RNA sequencing technique. We identified two novel endothelial cell (EC) populations characterized by either exosome synthesis and inflammation response, or vascular function and angiogenesis. Three osteoblast (OB) subtypes are introduced, separately related to vascularization, matrix manufacturing and matrix mineralization. The distinct roles and functions of these novel phenotypes in OA development are further discussed, as well as interaction network between these subpopulations. The variation tendency of each population is testified in a DMM mouse model. The identification of cell types demonstrates a novel taxonomy and mechanism for ECs and OBs inside subchondral bone area, provides new insights into the physiological and pathological behaviors of subchondral bone in OA pathogenesis.

Keywords: Osteoarthritis, subchondral bone, Single-cell RNA-seq, cell heterogeneity

Introduction

Osteoarthritis (OA) is an insidiously progressive, high-cost, and poorly prognostic joint disease, affecting approximately 250 million patients worldwide.[1] The most common clinical manifestations of OA are chronic cartilage degeneration, subchondral bone microstructure alteration, osteophyte formation, and intractable joint pain.[2-4] Fundamental research targeting articular cartilage destruction or cell senescence revealed considerable therapeutic potential of cartilage repair methods, however, the clinical trials have failed to varying degrees in recent decades.[5, 6] Accumulating evidence suggests that pathological alterations inside the subchondral bone are responsible for chondrocyte reduction and matrix degradation.[7, 8] The turnover rate of subchondral bone remains relatively low under normal circumstances and is accelerated by multiple factors in OA status, including mechanical and biological factors. The uncontrolled bone remodelling in the subchondral bone results in subsequent changes, including hypervascularisation, hyperpathia, abnormal mechanical support, and cartilage destruction.[9] Currently, both physiological and pathological behaviours of the subchondral bone have been valued in advanced research targeting OA therapies. However, the composition of subchondral bone cell types in patients with OA and the underlying spatiotemporal transformation processes remain unknown.

Mesenchymal stromal cells, osteoblasts (OBs), osteoclasts, endothelial cells (ECs), and immune cells are delicately orchestrated by various biological and mechanical factors in the local microenvironment of the subchondral bone.[9] Under abnormal loading conditions, the activated form of TGF-β is released from the bone matrix, resulting in aberrant vascularisation and osteogenesis.[10] Hypertrophic chondrocytes also participate in this

process as the major source of VEGF, coupled vessel invasion, cartilage remodelling, and ossification.[11] Interestingly, ECs recruited by multiple biological agents are the major driving forces of cartilage matrix degradation, bone elongation, and remodelling.[12] Moreover, OB-derived VEGF participates in the delicate bone-vessel crosstalk,[13] however, the specific communication mode inside the OA subchondral bone remains unknown. OBs have multiple functions, including angiogenesis promotion, matrix manufacturing and mineralisation.[14] Simultaneously, the participation of various immune cells leads to aggravated inflammation and subchondral bone disorders.[15] This indicates the importance of subchondral bone cells in OA progression, and the multifaceted nature of ECs and OBs suggests that they are comprised of diverse subpopulations. Nevertheless, considering the high phenotypic heterogeneity and limited understanding of biomarkers, the isolation and definition of EC and OB subtypes in human subchondral bone remains unclear.

To reveal the cellular interactions involved in the OA subchondral environment, single-cell RNA sequencing (scRNA-seq) was performed on tibial subchondral bone samples from patients undergoing total knee arthroplasty. Here, the scRNA-seq technique was utilised to map a general census of subchondral bone cells from both normal and OA sites, determine the genetic characteristics of these cell subgroups, and further analyse their potential differentiation relationships to characterise specific cell types. Finally, we investigated the cell-cell interaction network between EC and OB subpopulations. These results expand our understanding of the heterogeneity between patients and provide a theoretical basis for personalised OA therapies.

RESULTS

Single-cell profiling of human OA subchondral bone cells

To identify the cellular constitution of subchondral bone cells in human OA, we isolated human OA subchondral bone cells obtained from both lateral and medial tibial plateaus of two patients undergoing knee arthroplasty and profiled subchondral bone cells from different locations and patients (n=4) using scRNA-seq (Figure1A and supplementary Table S1). Through unbiased clustering of human subchondral bone cells, we found 10 clusters from OA patients were identified, including T (11151), B (990), NK (5155), NKT (7538), and dendritic cells (DCs; 124), monocytes and macrophages (557), bone-related cells (864): ECs (246), mesenchymal stem cells (MSCs; 104), and OBs (360). According to animal experiments and clinical experience, OA involvement is more common and occurs earlier in the medial side of the tibial plateau. In this study, we selected patients with severe medial destruction and an almost healthy lateral plateau. These two patients were fully informed of their condition and chose total knee arthroplasty. Subchondral bone cells were divided into the control group (Ctrl; 13024) from the lateral tibial plateau and the OA group (13355) from the medial side (Figure1B). In total, 26379 cells were retained for subsequent analysis after rigorous filtration (Figure1C, D; Supplementary FigureS1A, S2A and supplementary Table S2).

Next, the cell type distribution in the Ctrl and OA groups was analysed. In addition to the relationship between immune and myeloid cells, paired correlation analysis showed tight connections between ECs and MSCs, ECs and OBs, and MSCs and OBs (Figure1E). The first ten upregulated genes from these ten clusters were used to create a heatmap (Figure1F). Representative markers for T, B, NK, and NKT cells, DCs, monocytes, macrophages, ECs, MSCs,

and OBs were revealed (Figure1G). Specifically, the following clusters were identified: (1) B cells (expressing CD79A, BANK1, and MS4A1), (2) NK cells (expressing GZMB and NKG7), (3) NKT cells (expressing NKG7 and CD3D), (4) T cells (expressing CD3D and CD3G), (5) DCs (expressing LILRA4 and PTCRA), (6) monocytes (expressing CSTA and FCN1), (7) macrophages (expressing CD14, CD68, CSF1R, C1QC, and F13A1), (8) ECs (expressing PECAM1 and CLDN5), (9) MSCs (expressing MCAM), and (10) OBs (expressing RUNX2 and cadherin 11 [CDH11]; Figure1H and Supplementary FigureS1B, S2B–D).

Identification of bone-related cell populations in human OA subchondral bone

Abnormal angiogenesis, subchondral bone remodeling and sensory innervation are well recognized during early stage of OA, and might cause cartilage destruction and pain directly or indirectly.[13] Therefore, OBs, osteoclasts, ECs, and neuronal cells were the focus of our research, rather than immune cells. To define the cell subpopulation and identify genome-wide gene expression patterns, bone-related cells were clustered to produce eight clusters (Figure2A). Next, to explore the potential transformation between different cell types and visually depict the differentiation paths, the Monocle method was used to determine the pseudotemporal order between cell types (Figure2B, C). Our analysis clearly identified and verified three major groups of differentiated cell types: ECs (PECAM1+), MSCs (MCAM+), and OBs (RUNX2+/CDH11+; Figure2D).

Among the eight clusters, cluster1 expressed markers of multiple cell types, such as CTSK, RGS10, and SPP1, suggesting that cluster1 contains osteoclasts, nerve cells, and OBs (Supplementary Figure3). Cluster1 is a heterogeneous cell cluster; therefore, we only

102 analysed OBs, ECs, and MSCs. To determine the characteristics of each cell cluster by
103 analysing differential gene transcript expression patterns, a differentially expressed feature
104 analysis was performed using the scRNA-seq dataset and all cell clusters were compared with
105 one another. We discovered 78 differentially expressed genes (DEGs) that best divided
106 bone-related cells in subchondral bone into eight subclusters (Figure2E). Next, the original
107 sample information and expression levels of the indicated markers were combined to
108 determine the cell identity of each cluster, and their biological functions were analysed via
109 regulons CSI correlation heatmap of the co-expression between transcription factors (TFs)
110 and potential target genes. Seven major cell clusters were identified: precursor ECs, pre-ECs
111 (C2CD4B+/B3GNT5+); ECs (VWF+/KDR+); endothelial OBs, EnOBs (ABCA10+/microsomal
112 glutathione S-transferase 1 [MGST1]+); stromal OBs, StOBs (PTGS2+/
113 glutamine-fructose-6-phosphate transaminase 2 [GFPT2]+); mineralised OBs, MinOBs (WNT
114 inhibitory factor 1 [WIF1]+/NDNF+), and two MSC subpopulations (Figure2F–H). Through
115 SCENIC analysis, we discovered that pre-ECs and ECs exhibit activated pro-angiogenesis
116 regulons, such as SMAD1, ERG, and ETS1, and that the regulators have higher activity in ECs
117 than in pre-ECs. Furthermore, OB subpopulations exhibited similar activated TFs, however,
118 the regulatory activities of TFs are different (Figure2I, J).

119 **Identification of pre-ECs and ECs**

120 In addition to the well-known differences between arteries, capillaries, and veins, ECs
121 are highly heterogeneous and acquire specialised functional properties in the local
122 microenvironment. The articular cartilage is constantly maintained in a low-oxygen

123 environment. However, due to the high metabolic requirements of OBs, blood vessels are
124 required to provide sufficient oxygen. The cells are relatively hypoxic during osteogenesis.
125 Osteogenesis and nearby ECs may increase HIF-1α expression. Upregulation of HIF-1α
126 activity in hypoxic tissues leads to increased VEGF expression and promotes angiogenesis.
127 Using immunofluorescence and flow cytometry to identify the EC subpopulation in bone,
128 Kusumbe et al. proposed the following terminology for bone microvessels: H-type for the
129 small PECAM1^{hi}/Emcn^{hi} subset and L-type for the PECAM1^{lo}/Emcn^{lo} sinusoidal vessels.[16] As
130 previously mentioned, EC subpopulations were divided into pre-ECs and ECs, and we
131 discovered certain differences between them (Figure2E, F). To investigate the distinct
132 features of pre-ECs and ECs, we identified DEGs between them (Figure3A). The Gene
133 Ontology (GO) and Kyoto Encyclopaedia of Genes and Genomes (KEGG) were analysed with
134 these DEGs to show pre-EC and EC characteristics. Notably, pre-ECs were enriched for
135 extracellular exosomes, interleukin-mediated signalling pathways, and ribosomes, whereas
136 ECs were enriched for vasculogenesis, angiogenesis, EC migration, and signalling pathway
137 regulation, such as VEGF, Rap1, PI3K/Akt, Ras, and MAPK signalling pathways (Supplementary
138 FigureS4A–D). Then we compared characteristic genes of these two clusters Pre-EC
139 identification markers have diverse functions, including genes related to ribosome synthesis,
140 exosome synthesis, and inflammation, including RPL17, HNRNPF, RABA5, and C2CD4B,
141 whereas ECs are primarily enriched in genes related to angiogenesis, such as VWF, KDR, TIE1,
142 and CDH5 (Figure3B). Moreover, angiogenesis-related EMCN, PECAM1, EGFL7, ENG, and KDR
143 were all upregulated during the differentiation of pre-ECs to ECs, while exocrine-related
144 DDIT3 and RAB5A73 and inflammation-related CCL2 and C2CD4B74 were downregulated

(Figure3C).

Next, the essential motifs of the two EC subpopulations were identified using SCENIC analysis. As the specific motifs of pre-ECs, ATF3 and CEBPD are essential in the transcriptional regulation of inflammation, whereas ERG and SMAD1 motifs, which are closely related to angiogenesis, are highly activated in ECs. SOX17 and JunD are TFs that are widely expressed in pre-ECs and ECs (Figure3D and Supplementary FigureS5A,B). In a previous study, SMAD1 sprouted angiogenesis in human embryonic stem cell-derived ECs.[17] ERG is an essential regulator of angiogenesis and vascular stability through Wnt signalling.[18] These results may help us to identify pre-ECs and ECs and expand our understanding of the novel function of subchondral EC subsets in OA.

During OA progression, the EC cluster was a substantially increased cell population (Figure1E). To investigate the distinct features of the OA and Ctrl groups, we identified DEGs between these two groups in pre-ECs and ECs (Supplementary FigureS6A,B). To analyse the identified features of pre-EC and EC clusters from the OA group, we analysed the differences using GO, KEGG, and Gene Set Enrichment analyses (GSEA). Notably, compared with that of the Ctrl group, pre-ECs of the OA group showed stronger protein synthesis, inflammation-related pathways, and responses, whereas ECs were enriched for angiogenesis-promoting functions, such as blood vessel development, EC differentiation, and platelet-derived growth factor binding (Figure3E,F and Supplementary FigureS6C,D).

Determining the relationships among EnOBs, StOBs, and MinOBs

According to Rutkovskiy et al., OBs undergo a 3-stage differentiation: Stage 1, the cells

166 continue to proliferate; Stage 2, they start differentiating, while maturing the extracellular
167 matrix (ECM) with alkaline phosphatase (ALP) and collagen; and Stage 3, the matrix
168 mineralisation and mineral deposits increase.[19] According to the SCENIC analysis (Figure2I),
169 we found that the TF types and transcriptional activities were different among EnOBs, StOBs,
170 and MinOBs, which means that these clusters may have different cellular functions. By
171 identifying DEGs between EnOBs, StOBs, and MinOBs, the differences between OB
172 subpopulations were further verified (Figure4A). To explain the specific characteristics of
173 these three OB populations, we analysed the differences through GO and KEGG analyses.
174 EnOBs are related to EC migration, VEGF binding, and the PDGFR-β signalling pathway, and
175 express NRP1, PDGFRB, and VCAM, suggesting that this cluster may have potentially affect
176 angiogenesis. StOBs were enriched for collagen and fiber-related biological processes, such
177 as collagen fibril organisation, fibronectin binding, and ECM binding. MinOBs distinctively
178 expressed an ossification and bone mineralisation biological process gene signature
179 (Figure4B and Supplementary FigureS7A–C). Next, representative candidate markers among
180 EnOBs, StOBs, and MinOBs (Figure4C) were identified, including TFs (Figure4F).

181 Next, the Monocle method was applied to depict the pseudotemporal sequence of
182 potential differentiation pathways among cell types. According to the pseudotime trajectory
183 axis, we suggest that StOB is an intermediate state representing the state between EnOBs
184 and MinOBs (Figure4D,E). The pseudotemporal expression dynamics of representative
185 candidate markers and TFs also marked the progression from EnOBs to StOBs to MinOBs.
186 Through SCENIC analysis, we found that TFs upregulated by EnOBs were related to
187 angiogenesis, such as MECOM, ERG, and XBP1, and TFs related to collagen and fibre in StOBs,

188 including FOSL2, ERG1, and ATF4, and VDR and FOXC2 in MinOBs are related to
189 mineralisation (Figure4F and Supplementary FigureS8A–C). Taken together, these data reveal
190 the relationships and potential functions of EnOBs, StOBs, and MinOBs.

191 The number of OBs increased in abundance during OA progression, more so than in ECs
192 (Figure1E). To investigate the distinct features of normal and diseased cells inside the
193 subchondral zone, we identified DEGs between the OA and Ctrl groups of these three OB
194 clusters, respectively (Supplementary FigureS9A–C). We then analysed the differences by
195 GSEA and GO analysis. Notably, compared with that of the Ctrl group, the OA group of EnOBs
196 showed stronger angiogenesis and wound healing biological processes; the OA group of
197 StOBs was enriched for ECM binding and collagen fibril organisation, and the OA group of
198 MinOBs was enriched for response of metal ions such as cadmium, copper, and zinc
199 (Figure4G,H). Regarding these ionic reactions, copper ions in biological materials promote
200 bone formation,[20] zinc increases OB activity and collagen synthesis,[21] and cadmium promotes
201 OB differentiation.[22] These results indicate that OBs in the OA group have stronger
202 osteogenic effects and we will further verify the functional heterogeneity of the three OB
203 subpopulations.

204 **Vascular EC and OB subpopulation interaction**

205 Through the interaction of H-type blood vessels and various cytokines in bone
206 metabolism, angiogenesis and bone formation are precisely coupled.[16] MSCs are chemically
207 recruited by ECs to promote osteogenesis.[23] Furthermore, the crucial signalling pathways in
208 MSCs coupled with ECs include the TGF-β, PDGF-PDGFR, angiopoietin, Notch, and FAK

209 signalling pathways. To further explore the key signalling pathway that couples OBs and ECs,
210 we studied the cell-cell interaction network between the identified clusters. Considering the
211 outcomes of GSEA and GO enrichment analyses and the characteristics of the genes and TFs,
212 we chose to analyse the interaction pairs, including chemokines, ephrin receptor family,
213 NOTCH family, cytokines, and integrins. We found that ECs were the predominant cell
214 population interacting with the OB subpopulation, and pairwise correlation analysis revealed
215 that ECs are more closely related than pre-ECs to OB subpopulations (Figure5A, B).

216 Compared with pre-ECs, ECs express a larger number of membrane receptors,
217 fibronectin and collagen, and secrete a larger number of angiocrine factors. EC analysis
218 revealed that ECs exhibited abundant expression of multiple membrane receptors for ligands
219 important for vascular development, including NOTCH1, NOTCH4, VEGF receptors (KDR, FLT1,
220 FLT4, NRP1, NRP2), TGFβ receptors (TGFBR3), ephrin B receptor (EPHB4), and tyrosine kinase
221 receptor (TEK), which bind to JAG1, the VEGF family, PGF, ANGPT1, and TGFβ 1 ligand
222 secreted by OB to promote angiogenesis (Figure5C–E and Supplementary FigureS10A–C).
223 These results indicate that ECs are a mature EC subgroup with angiogenic function at the
224 transcriptional level, and are mainly coupled with OBs. Notably, pre-ECs hardly secrete any
225 ligands, as the results showed, however, considering the enrichment analysis data of pre-ECs
226 (Supplementary FigureS4A), we hypothesise that the function of pre-ECs is achieved by
227 secreting exosomes, which requires further investigation.

228 There is little difference between chemokine interaction pairs in OBs, and they all
229 express CXCR4 to promote OB proliferation and differentiation, however, only MinOBs do not
230 secrete CXCL12.[24] At the end of osteogenic differentiation, CXCL12 is downregulated.[25] We

found that the overall expression of the ephrin receptor and NOTCH family members decreased gradually from EnOBs to StOBs to MinOBs. The ephrin receptor[26] and NOTCH families[27] promote OB proliferation, and the lack of the bone system JAG1 leads to mature OB proliferation, which is manifested as an increase in the rate of mineral deposition (Figure5F). Additionally, we found that these three OB subgroups are affected by bone morphogenetic proteins, which have a strong positive effect on bone formation.[28] PGF, PDGF, and VEGF families secreted by ECs and OBs could interact with the receptors highly expressed on the surface of EnOBs, including NRP1, PDGFRA, and PDGFRB. These cytokines are related to angiogenesis, and PDGF induces OB proliferation via the ERK signalling pathway.[29] We also found that TGFβ1 was produced by all three types of OBs, but only bound with TGFβ receptors on EnOBs to play a role in promoting OB proliferation,[30] inducing VEGF secretion[31] and inhibiting mineralisation function.[32] As a non-collagenous protein in the bone ECM that is recognised to regulate bone formation and mineralisation, osteopontin (OPN/SPP1) is expressed and released in the integrin interaction pair by MinOBs only (Figure5G, H). Compared with that of EnOBs and MinOBs, StOBs expressed the highest fibrin and collagen levels, while MinOBs expressed the lowest (Figure5H). In summary, the above data further validated our understanding of the role of these five major cell clusters in bone-associated cells and the interaction between ECs and OBs.

Pathological identification of subpopulations

In order to further verify our sequence results, we conducted destabilisation of the medial meniscus (DMM) surgery on 6-week-old C57B6J mice, simulating patient conditions

252 before arthroplasty surgery (Figure6A). The tibial subchondral bone volume in OA mice
253 showed significant changes after surgery, as shown by microCT, safranin O, fast green
254 staining, and H&E staining (Figure6B). The total tissue volume of subchondral bone
255 decreased at 2 weeks and increased at 4 weeks post-surgery, and the subchondral bone
256 structure densified at 8 weeks (Figure6C). Microstructure disruption was indicated by
257 aberrant subchondral bone plate thickness and trabecular pattern factor, according to the
258 microCT calculation (Figure6C). Osteoarthritis Research Society International scores indicated
259 that cartilage degeneration was significant at 4 weeks and deteriorated at 8 weeks
260 post-surgery (Figure6D).

261 An immunofluorescence test was performed to characterise cell development and
262 trajectory during OA pathology. The ratio of ECs among the total PECAM1-positive cells
263 increased continuously after surgery (Figure7A). Specifically, PECAM1-positive ECs were
264 rather rare and were near the trabecular before intervention, indicating a relatively low
265 angiogenesis rate. An important proportion of PECAM1-positive cells were KDR-negative, or
266 pre-ECs, in the sham group (66.4±9.44%) and 0w samples in the DMM group (60.69±8.77%).
267 They are characterised by genes coded for ribosome synthesis, extracellular vesicles
268 synthesis, and inflammation, indicating hypermetabolism and pro-inflammatory status inside
269 the subchondral bone. ECs grew more after 4 weeks and the ratio of KDR-positive, or ECs
270 with relatively high angiogenesis trends, increased significantly and reached 82.97±8.01%.
271 With severe subchondral sclerosis progression, the majority (88.90±4.62%) of ECs became
272 pre-ECs, and the total number of pre-ECs and ECs decreased dramatically in the limited space
273 (Figure7B).

Next, we analysed the OB subpopulation marked by osteocalcin (OCN), MGST1, GFPT2, and WIF1. Consistent with previous results, the total number of OCN-positive cells increased during the first 4 weeks and decreased at 8 weeks post-surgery (Figure7C). Analogously, EnOBs characterised by angiogenesis-related genes increased dramatically 2 weeks post-DMM surgery and decreased at 8 weeks (Figure7D, top). StOBs capable of ECM binding and collagen fibril organisation increased continuously during the first 4 weeks post-trauma and decreased at 8 weeks (Figure7D, middle), probably because of the calcification requirement. MinOBs, which were closely related to metal ion and biomineralisation, increased dramatically at 8 weeks post-surgery and accounted for approximately 48% of the total OCN-positive cells (Figure7D, bottom). Taken together, these data indicate chronological changes in OB subgroups and mapping the over-time changing bio-function of OBs in subchondral bone during post-traumatic OA.

Discussion

OA is one of the most common degenerative diseases that cause disability in older adults. An epidemiological study by Tang et al. showed that 8.1% of the adult population had clinically significant OA of the knee or hip.[33] Moreover, OA consumes a substantial amount of healthcare resources, primarily owing to the joint replacement surgery costs for advanced OA.[33] Increasing economic pressure, an aging society, and the obesity epidemic emphasise the need for new strategies for the diagnosis and intervention at early-stage OA.[34-36] Increasing evidence suggests that the appearance of subchondral bone lesions occurs earlier than cartilage degeneration, and the pathological alterations of subchondral bone play an

important role in OA development. During the initial phase of OA, the bone turnover rate beneath the articular cartilage was upregulated, and vascular invasion took place bottom-up from the subchondral, the tidemark, and ultimately into the cartilage. Since the exact role of subchondral bone during OA initiation and progression remains unclear, and the specific cell markers are lacking, it is urgent to unveil the internal state of subchondral bone cells in OA pathogenesis. Here, we used comprehensive gene expression profiling to reveal the cell types that make up the subchondral bone microenvironment at single-cell resolution, and also novel cell markers and characteristics to verify each hypothetical subchondral bone cell cluster.

We identified 10 different cell types in the human OA subchondral bone microenvironment. Notably, there were more OBs and ECs in the OA group than in the Ctrl group. This finding validates the characteristics of increased bone formation and angiogenesis in OA subchondral bone.[37] In addition to the empirically inferred subchondral bone cell types, we identified new subtypes of bone-associated cells and new markers of bone-associated cell populations based on scRNA-seq analysis. Based on the expression of TFs and markers of the new subtypes, we suggest that EC subtypes and OB subtypes perform different biological functions.

In the process of OA cartilage erosion, compared with the top-down vessel invasion originating from synovial tissue or synovium, bottom-up vascularization from subchondral bone plays a larger role.[38] In the process of bone elongation, ECs constantly erode the cartilage matrix, thus creating space for osteogenesis. Kusumbe et al. identified two types of special blood vessel subtypes based on the expression strength of PECAM1 and EMCN,

317 namely H-type (PECAM1^{hi}EMCN^{hi}) and L-type blood vessels (PECAM1^{lo}EMCN^{lo}).[16] In the
318 present study, we also identified two EC phenotypes: pre-ECs and ECs. We found that
319 PECAM1 and EMCN expression in ECs was upregulated, suggesting that it may have functions
320 similar to those of H-type blood vessels. By comparing gene expression, TF activity, and
321 enrichment analysis, we suggest that the “ECs” in this research are a type of endothelial cells
322 that promote angiogenesis, and can also be coupled with OBs. In this study, we identified a
323 new subset named pre-ECs, characterised by interleukin-mediated inflammation pathways
324 and exosomes. A key element leading to the advancement of OA is the production of high
325 inflammatory cytokine levels, and the pro-inflammatory cytokine interleukin 1β (IL-1β) is
326 expressed in large quantities during OA. Elevated IL-1β levels are associated with tissue
327 damage and reflect the severity of inflammation. During subchondral bone reconstruction,
328 IL-1β may also play a role in promoting cartilage calcification (ossification) and cartilage
329 degeneration.[39] Yang et al. showed that exosomes derived from vascular ECs promoted the
330 progression of OA by promoting chondrocyte apoptosis.[40] Therefore, we speculate that
331 pre-ECs in OA may allow for bone formation through exosomes digesting cartilage and
332 promote subchondral bone remodelling through IL-mediated inflammation. The
333 characterisation of these two novel subsets improves our understanding of the
334 characteristics and functions of ECs in the OA subchondral bone.

335 Subchondral bone sclerosis is characterised by an increase in bone volume due to an
336 enhanced bone turnover rate.[37] In the OA subchondral bone, we found three OB phenotypes:
337 EnOBs, StOBs, and MinOBs. We believe that EnOBs are enriched in angiogenesis-related
338 pathways, StOBs are characterised by collagen and fibrosis, and MinOBs specifically express

339 mineralization-related markers. Here, we found that the three OB phenotypes have a
340 differentiation path, from EnOBs to StOBs to MinOBs. The first stage of OB differentiation is
341 characterised by cell proliferation. EnOBs are tightly correlated with vascularisation,
342 including EC migration, VEGF binding, and platelet-derived growth factor receptor β (PDGFRβ)
343 signalling pathways. Angiogenesis directly promotes bone formation, and CDH11 cooperates
344 with PDGFRβ to promote cell proliferation. In the next stage, OBs begin to differentiate and
345 express collagen and alkaline phosphatase ALP. StOBs are OBs characterised by OB
346 differentiation and collagen fibril organisation, and express high levels of fibulin-1 (FBLN1),
347 collagen type XI alpha 1 (COL11A1), and PLOD2. FBLN1 is an important ECM protein that
348 stabilises collagen and other ECM proteins. COL11A1, as one of the three alpha chains of
349 type XI collagen, is critical for collagen fiber assembly and bone development. OA-related
350 fibrosis is associated with elevated PLOD2 expression.[41] In the last stage, OBs express
351 markers of more bone sialoprotein, OPN/SPP1, and osteocalcin (BGLAP), thereby inducing
352 matrix mineralisation. In this study, we found that MinOBs specifically express the
353 above-mentioned mature OB phenotypic markers, representing the biological processes of
354 ossification, bone mineralisation, and biomineral tissue development. Additionally, MinOBs
355 express the Wnt antagonist WIF1, which regulates the Wnt/β-catenin signalling pathway to
356 reduce cell proliferation and promote mineralisation.[42]

357 The coupling of osteogenesis and angiogenesis causes increased bone mineral density
358 and significant microstructural changes in the subchondral bone. Through the analysis of
359 cell-to-cell communication between ECs and OBs, we found that ECs with angiogenic
360 function and upregulated PECAM1 and EMCN expression are coupled with OBs through

NOTCH, VEGF, and TGFβ receptors, EPHB4, and TEK. Although we highlighted the role of ECs in cell-to-cell communication instead of pre-ECs, the contribution of pre-ECs in the advancement of OA could not be neglected. We found that specific receptors on OBs, including EPH, NOTCH, BMPR, NRP, PDGFR, TGFβR, fibronectin, collagen, and SPP1 (OPN), responded to signals derived from ECs, thus further elucidating the interaction between the osteogenic subgroups and ECs. Furthermore, EnOBs are related to angiogenesis and promote OB proliferation. StOBs express higher levels of fibrin and collagen. Moreover, OPN, which is directly related to mineralisation, is expressed only by MinOBs.

In conclusion, our scRNA-seq analysis results provided a clearer and more consistent definition of the cellular components of human subchondral bone in OA. Specifically, two novel populations of ECs and three subpopulations of OBs, as well as the intercellular interaction network between these subpopulations, were identified. Our analysis provides new insights into the physiological and pathological behaviours of subchondral bone in OA pathogenesis, which may contribute to novel therapeutic strategies in the future.

Materials and Methods

Human subchondral bone samples were collected during total knee arthroplasty operations. Bone samples were cut into 1–2 mm pieces and then digested in 0.2% type II collagenase (17101015, Thermo Fisher Scientific, MA, USA) for 2 h. Cells were then collected after red blood cell lysis.

Raw data processing and quality control The Cell Ranger software pipeline (version 3.1.0) provided by 10× Genomics was used to demultiplex cellular barcodes, map reads to the

382 genome and transcriptome using the STAR aligner, and down-sample reads as required to
383 generate normalized aggregate data across samples, producing a matrix of gene counts
384 versus cells. We processed the unique molecular identifier (UMI) count matrix using the R
385 package Seurat (version 3.0). To remove low quality cells and likely multiplet captures, which
386 is a major concern in microdroplet-based experiments, we apply a criteria to filter out cells
387 with UMI/gene numbers out of the limit of mean value +/- 2 fold of standard deviations
388 assuming a Guassian distribution of each cells' UMI/gene numbers. Following visual
389 inspection of the distribution of cells by the fraction of mitochondrial genes expressed, we
390 further discarded low-quality cells where a certain percentage of counts belonged to
391 mitochondrial genes. Library size normalization was performed in Seurat on the filtered
392 matrix to obtain the normalized count.
393 Top variable genes across single cells were identified using the method described in Macosko
394 et al. Briefly, the average expression and dispersion were calculated for each gene, genes
395 were subsequently placed into several bins based on expression. Principal component
396 analysis (PCA) was performed to reduce the dimensionality on the log transformed
397 gene-barcode matrices of top variable genes. Cells were clustered based on a graph-based
398 clustering approach, and were visualized in 2-dimension using tSNE. Likelihood ratio test that
399 simultaneously test for changes in mean expression and in the percentage of expressed cells
400 was used to identify significantly differently expressed genes between clusters. Here, we use
401 the R package SingleR, a novel computational method for unbiased cell type recognition of
402 scRNA-seq to infer the cell of origin of each of the single cells independently and identify cell
403 types.

Differentially expressed genes(DEGs) were identified using the Seurat package.p value < 0.05 and |log2foldchange| > 1 (or |log2foldchange| > 0.58) was set as the threshold for significantly differential expression. GO enrichment and KEGG pathway enrichment analysis of DEGs were respectively performed using R based on the hypergeometric distribution.

Pseudotime analysis Pseudotime analysis was performed with Monocle2 to determine the dramatic translational relationships among cell types and clusters. Further detection with the Monocle2 plot_pseudotime_heatmap function revealed the key role of a series of genes in the differentiation progress. Signifcantly changed genes were identified by the differential GeneTest function in Monocle2 with a q-value < 0.01.

Cell–cell communication analysis with CellPhoneDB 2 CellPhoneDB 2 is a Python-based computational analysis tool developed by Roser Vento-Tormo et al, which enables analysis of cell–cell communication at the molecular level. A website version was also provided for analysis of a relatively small dataset (http://www.cellphonedb.org/). As described above, 606 single cells that were clustered into 5 cell types were investigated using the software to determine interaction networks. Interaction pairs including chemokines, ephrin receptor family, NOTCH family, cytokines and integrins and have p-values < 0.05 returned by CellPhoneDB, were selected for the evaluation of relationships between cell types.

SCENIC analysis SCENIC is a new computational method used in the construction of regulatory networks and in the identification of different cell states from scRNA-seq data. To

measure the difference between cell clusters based on transcription factors or their target genes, SCENIC was performed on all single cells, and the preferentially expressed regulons were calculated by the Limma package. Only regulons significantly upregulated or downregulated in at least one cluster, with adj. p-value < 0.05, were involved in further analysis.

Animal models Destabilization of the medial meniscus (DMM) or sham operations were conducted bilaterally on 6-week-old male C57B6J mice (n=5 in each group). Samples were harvested at 0, 2, 4 and 8 weeks after surgery. Mice of 0 weeks were conducted with sham operation. Hearts were perfused with PBS and 4% PFA successively in order to fix the antigens. Bilateral knee joints were harvested and fixed in 4% PFA for 24 hours, then went through micro-CT scan (60kV, 50μA, 10 um pixel).

Pathological staining Samples were decalcified in 10% EDTA for two weeks, paraffin sections of 6 μm were then prepared for subsequent experiments: HE, safranin O and fast green (SOFG) and immunofluorescence (IF) staining. HE and SOFG staining experiments were conducted under manufacturer's instructions (Beyotime, C0105M; Solarbio, G1371). Antibodies utilized during IF staining: Rat anti Mouse PECAM1 (Thermo fisher, 140311-82); Rabbit anti Mouse KDR (Abcam, ab11805); Rat anti Mouse OCN (Takara, M188); Rabbit anti Mouse MGST1 (Abcam, ab131059); Rabbit anti Mouse GFPT2 (Abcam, ab190966); Rabbit anti Mouse WIF1 (Santa, sc-373780); Goat anti Rat secondary antibody (Abcam, ba150165); Goat anti Rabbit secondary antibody (Abcam, ab150080). Nuclei were marked by DAPI

(Beyotime, C1002).

Statistical analysis Statistical calculations were performed using R package and GraphPad Prism (version 9.3). The results of microCT and staining are presented using line charts. The two-way ANOVA was applied to identify differences between groups in statistical graphs. Results were considered statistically significant when $p < 0.05$.

Acknowledgements

We thank OE biotech company (Shanghai, China) for the support of bioinformatics analysis. This work is supported by National Key R&D Program of China (2018YFC2001500), National Natural Science Foundation of China (82172098).

Author contributions

Conceptualization: JCS, XC, KX; Methodology: YH, JC, HL, SCW; Investigation: YH, KX, HL; Visualization: KX, YH; Supervision: JCS, LHC; Writing—original draft: YH, KX; Writing—review & editing: JCS, XC.

Competing interests

None declared.

Ethics approval

Protocol approved by the Ethical Committee of Shanghai University (ECSHU 2021-146).

References

1. Hunter, D. J., and Bierma-Zeinstra, S. (2019). Osteoarthritis. Lancet (London, England) 393: 1745-1759.

2. Edwards, J. J., Khanna, M., Jordan, K. P., Jordan, J. L., Bedson, J., and Dziedzic, K. S. (2015). Quality indicators for the primary care of osteoarthritis: A systematic review. Ann. Rheum. Dis. 74: 490-498.

3. Kim, J., Jeon, J., Shin, M., Won, Y., Lee, M., Kwak, J., Lee, G., Rhee, J., Ryu, J., and Chun, C., et al. (2014). Regulation of the catabolic cascade in osteoarthritis by the zinc-ZIP8-MTF1 axis. Cell 156: 730-743.

4. Wang, T. Y., and Chen, D. (2016). Differential roles of TGF- β signalling in joint tissues during osteoarthritis development., p. e72.

5. Childs, B. G., Gluscevic, M., Baker, D. J., Laberge, R., Marquess, D., Dananberg, J., and van Deursen, J. M. (2017). Senescent cells: An emerging target for diseases of ageing. Nature reviews. Drug discovery 16: 718-735.

6. Pitsillides, A. A., and Beier, F. (2011). Cartilage biology in osteoarthritis--lessons from developmental biology. Nature reviews. Rheumatology 7: 654-663.

7. Goldring, S. R., and Goldring, M. B. (2016). Changes in the osteochondral unit during osteoarthritis: Structure, function and cartilage-bone crosstalk. Nature reviews. Rheumatology 12: 632-644.

8. Burr, D. B., and Gallant, M. A. (2012). Bone remodelling in osteoarthritis. Nature reviews. Rheumatology 8: 665-673.

9. Hu, Y., Chen, X., Wang, S., Jing, Y., and Su, J. (2021). Subchondral bone microenvironment in

482 osteoarthritis and pain. Bone Res 9: 20.

483 10. Zhen, G., Wen, C., Jia, X., Li, Y., Crane, J. L., Mears, S. C., Askin, F. B., Frassica, F. J., Chang,
484 W., and Yao, J., et al. (2013). Inhibition of TGF-β signaling in mesenchymal stem cells of subchondral
485 bone attenuates osteoarthritis. Nat. Med. 19: 704-712.

486 11. Gerber, H. P., Vu, T. H., Ryan, A. M., Kowalski, J., Werb, Z., and Ferrara, N. (1999). VEGF
487 couples hypertrophic cartilage remodeling, ossification and angiogenesis during endochondral bone
488 formation. Nat. Med. 5: 623-628.

489 12. Romeo, S. G., Alawi, K. M., Rodrigues, J., Singh, A., Kusumbe, A. P., and Ramasamy, S. K.
490 (2019). Endothelial proteolytic activity and interaction with non-resorbing osteoclasts mediate bone
491 elongation. Nat. Cell Biol. 21: 430-441.

492 13. Hu, K., and Olsen, B. R. (2016). Osteoblast-derived VEGF regulates osteoblast differentiation and
493 bone formation during bone repair. The Journal of clinical investigation 126: 509-526.

494 14. Ansari, N., and Sims, N. A. (2020). The cells of bone and their interactions. Handbook of
495 experimental pharmacology 262: 1-25.

496 15. Weber, A., Chan, P. M. B., and Wen, C. (2019). Do immune cells lead the way in subchondral
497 bone disturbance in osteoarthritis? Progress in biophysics and molecular biology 148: 21-31.

498 16. Kusumbe, A. P., Ramasamy, S. K., and Adams, R. H. (2014). Coupling of angiogenesis and
499 osteogenesis by a specific vessel subtype in bone. Nature 507: 323-328.

500 17. Liu, M., Zhang, L., Marsboom, G., Jambusaria, A., Xiong, S., Toth, P. T., Benevolenskaya, E. V.,
501 Rehman, J., and Malik, A. B. (2019). Sox17 is required for endothelial regeneration following
502 inflammation-induced vascular injury. Nat Commun 10: 2126.

503 18. Birdsey, G. M., Shah, A. V., Dufton, N., Reynolds, L. E., Osuna Almagro, L., Yang, Y., Aspalter, I.

504 M., Khan, S. T., Mason, J. C., and Dejana, E., et al. (2015). The endothelial transcription factor ERG
505 promotes vascular stability and growth through Wnt/ β -catenin signaling. Dev. Cell 32: 82-96.
506 19. Rutkovskiy, A., Stensløkken, K., and Vaage, I. J. (2016). Osteoblast differentiation at a glance.
507 Medical science monitor basic research 22: 95-106.
508 20. Shi, F., Liu, Y., Zhi, W., Xiao, D., Li, H., Duan, K., Qu, S., and Weng, J. (2017). The synergistic
509 effect of micro/nano-structured and Cu(2+)-doped hydroxyapatite particles to promote osteoblast
510 viability and antibacterial activity. Biomedical materials (Bristol, England) 12: 35006.
511 21. Gaffney-Stomberg, E. (2019). The Impact of Trace Minerals on Bone Metabolism. Biol. Trace
512 Elem. Res. 188: 26-34.
513 22. Ma, Y., Ran, D., Zhao, H., Song, R., Zou, H., Gu, J., Yuan, Y., Bian, J., Zhu, J., and Liu, Z. (2021).
514 Cadmium exposure triggers osteoporosis in duck via P2X7/PI3K/AKT-mediated osteoblast and
515 osteoclast differentiation. The Science of the total environment 750: 141638.
516 23. Carmeliet, P., and Jain, R. K. (2011). Molecular mechanisms and clinical applications of
517 angiogenesis. Nature 473: 298-307.
518 24. Verheijen, N., Suttorp, C. M., van Rheden, R. E. M., Regan, R. F., Helmich, M. P. A. C.,
519 Kuijpers-Jagtman, A. M., and Wagener, F. A. D. T. (2020). CXCL12-CXCR4 interplay facilitates
520 palatal osteogenesis in mice. Frontiers in cell and developmental biology 8: 771.
521 25. Ito, H. (2011). Chemokines in mesenchymal stem cell therapy for bone repair: A novel concept of
522 recruiting mesenchymal stem cells and the possible cell sources. Mod Rheumatol 21: 113-121.
523 26. Abeynayake, N., Arthur, A., and Gronthos, S. (2021). Crosstalk between skeletal and neural
524 tissues is critical for skeletal health. Bone 142: 115645.
525 27. Yu, J., and Canalis, E. (2020). Notch and the regulation of osteoclast differentiation and function.

526 Bone 138: 115474.

527 28. Lawal, R. A., Zhou, X., Batey, K., Hoffman, C. M., Georger, M. A., Radtke, F., Hilton, M. J.,

528 Xing, L., Frisch, B. J., and Calvi, L. M. (2017). The notch ligand jagged1 regulates the osteoblastic

529 lineage by maintaining the osteoprogenitor pool. Journal of bone and mineral research : the official

530 journal of the American Society for Bone and Mineral Research 32: 1320-1331.

531 29. Kinoshita, H., Orita, S., Inage, K., Fujimoto, K., Shiga, Y., Abe, K., Inoue, M., Norimoto, M.,

532 Umimura, T., and Ishii, T., et al. (2020). Freeze-Dried Platelet-Rich plasma induces osteoblast

533 proliferation via Platelet-Derived growth factor Receptor-Mediated signal transduction. Asian spine

534 journal 14: 1-8.

535 30. Zhang, Z., Zhang, X., Zhao, D., Liu, B., Wang, B., Yu, W., Li, J., Yu, X., Cao, F., and Zheng, G.,

536 et al. (2019). TGF - β 1 promotes the osteoinduction of human osteoblasts via the

537 PI3K/AKT/mTOR/S6K1 signalling pathway. Mol Med Rep 19: 3505-3518.

538 31. Ding, A., Bian, Y., and Zhang, Z. (2020). SP1/TGF - β 1/SMAD2 pathway is involved in

539 angiogenesis during osteogenesis. Mol Med Rep 21: 1581-1589.

540 32. Nam, B., Park, H., Lee, Y. L., Oh, Y., Park, J., Kim, S. Y., Weon, S., Choi, S. H., Yang, J., and Jo,

541 S., et al. (2020). TGF β 1 suppressed matrix mineralization of osteoblasts differentiation by regulating

542 SMURF1-C/EBP β -DKK1 axis. Int. J. Mol. Sci. 21.

543 33. Tang, X., Wang, S., Zhan, S., Niu, J., Tao, K., Zhang, Y., and Lin, J. (2016). The prevalence of

544 symptomatic knee osteoarthritis in china: Results from the china health and retirement longitudinal

545 study. Arthritis & rheumatology (Hoboken, N.J.) 68: 648-653.

546 34. Prieto-Alhambra, D., Javaid, M. K., Judge, A., Maskell, J., Cooper, C., and Arden, N. K. (2015).

547 Hormone replacement therapy and mid-term implant survival following knee or hip arthroplasty for

548 osteoarthritis: A population-based cohort study. Ann. Rheum. Dis. 74: 557-563.

549 35. Pan, F., Ding, C., Winzenberg, T., Khan, H., Martel-Pelletier, J., Pelletier, J., Cicuttini, F., and
550 Jones, G. (2016). The offspring of people with a total knee replacement for severe primary knee
551 osteoarthritis have a higher risk of worsening knee pain over 8 years. Ann. Rheum. Dis. 75: 368-373.

552 36. Schnitzer, T. J., Ekman, E. F., Spierings, E. L. H., Greenberg, H. S., Smith, M. D., Brown, M. T.,
553 West, C. R., and Verburg, K. M. (2015). Efficacy and safety of tanezumab monotherapy or combined
554 with non-steroidal anti-inflammatory drugs in the treatment of knee or hip osteoarthritis pain. Ann.
555 Rheum. Dis. 74: 1202-1211.

556 37. Hügle, T., and Geurts, J. (2017). What drives osteoarthritis?-synovial versus subchondral bone
557 pathology. Rheumatology (Oxford, England) 56: 1461-1471.

558 38. Moses, M. A., Sudhalter, J., and Langer, R. (1990). Identification of an inhibitor of
559 neovascularization from cartilage. Science (New York, N.Y.) 248: 1408-1410.

560 39. Chien, S., Tsai, C., Liu, S., Huang, C., Lin, T., Yang, Y., and Tang, C. (2020). Noggin inhibits
561 IL-1β and BMP-2 expression, and attenuates cartilage degeneration and subchondral bone destruction
562 in experimental osteoarthritis. Cells-Basel 9.

563 40. Yang, R., Zheng, H., Xu, W., Zheng, X., Li, B., Jiang, L., and Jiang, S. (2021). Vascular
564 endothelial cell-secreted exosomes facilitate osteoarthritis pathogenesis by promoting chondrocyte
565 apoptosis. Aging 13: 4647-4662.

566 41. Remst, D. F. G., Blaney Davidson, E. N., Vitters, E. L., Blom, A. B., Stoop, R., Snabel, J. M.,
567 Bank, R. A., van den Berg, W. B., and van der Kraan, P. M. (2013). Osteoarthritis-related fibrosis is
568 associated with both elevated pyridinoline cross-link formation and lysyl hydroxylase 2b expression.
569 Osteoarthr. Cartilage 21: 157-164.

570 42. Parra-Torres, A. Y., Enríquez, J., Jiménez-Ortega, R. F., Patiño, N., Castillejos-López, M. D. J.,

571 Torres-Espíndola, L. M., Ramírez-Salazar, E. G., and Velázquez-Cruz, R. (2020). Expression profiles

572 of the Wnt/β-catenin signaling-related extracellular antagonists during proliferation and differentiation

573 in human osteoblast-like cells. Exp Ther Med 20: 254.

Figure legends

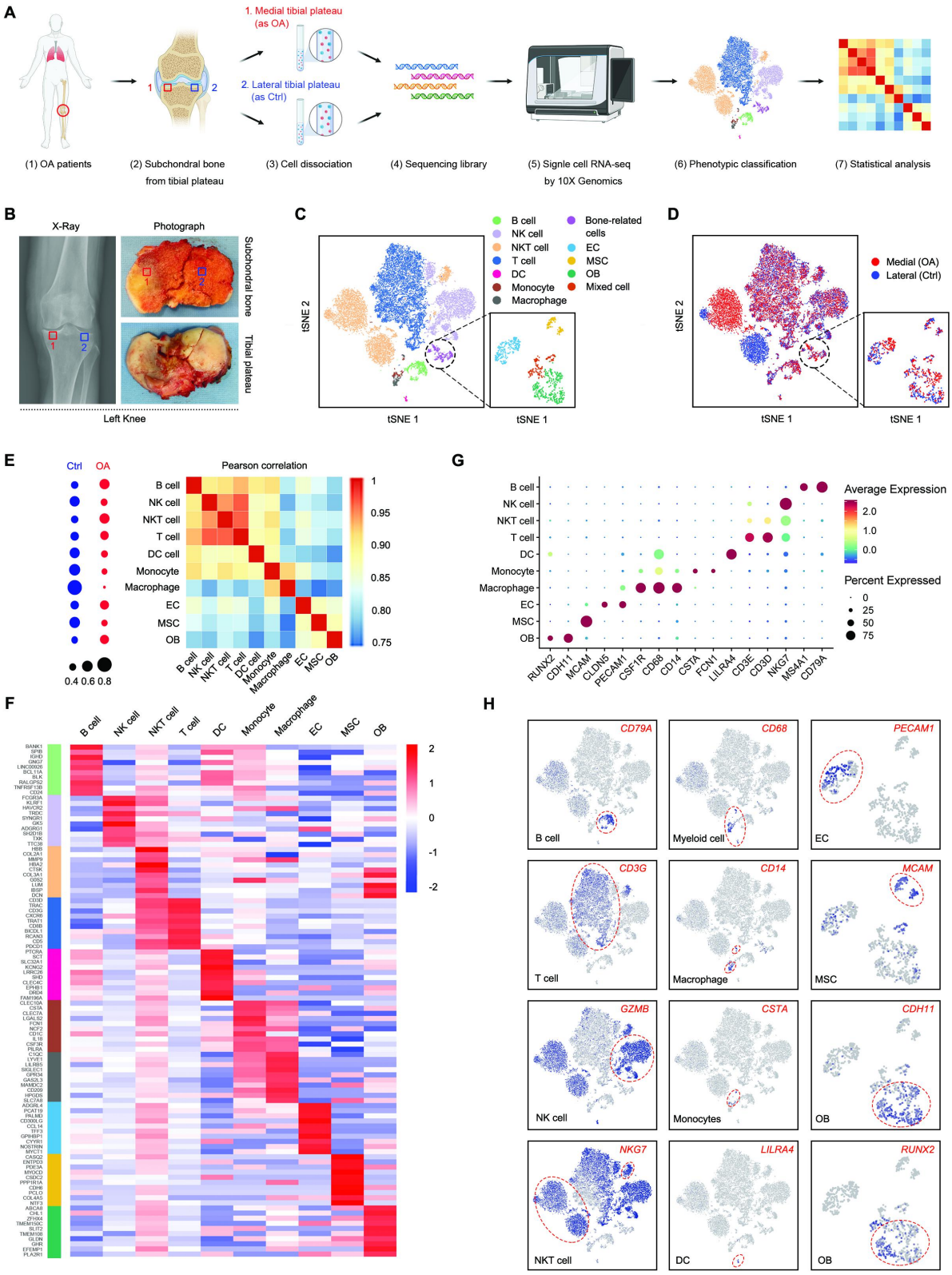

Figure1. Single-cell profiling of human OA subchondral bone cells

577 (A) Schematic workflow of the experimental strategy. (B) X-ray photograph of a patient with
578 knee osteoarthritis (OA; left) and corresponding cross-sectional anatomy of the
579 subchondral bone and tibial plateau (right). (C,D)The tSNE plots (left panel) and the sample
580 origin (right panel) of 26,379 subchondral bone cells and 864 bone-associated cells. (E) Dot
581 plots showing the distribution of each cell type in the control (Ctrl) and OA groups.
582 Heatmap showing the pairwise correlations. (F) Cluster averaged log-normalised expression
583 of the top 10 marker genes between the 10 cell types with stromal-related genes of interest
584 annotated. Expression values are scaled per cluster. (G) Dot plot showing the expression of
585 specific signatures in identified cell types in (F). The dot colour and size represent the mean
586 expression and proportion of each cell population expressing genes, respectively. (H)
587 Feature plots showing the expression of indicated markers for each cell type on the t-SNE
588 map.

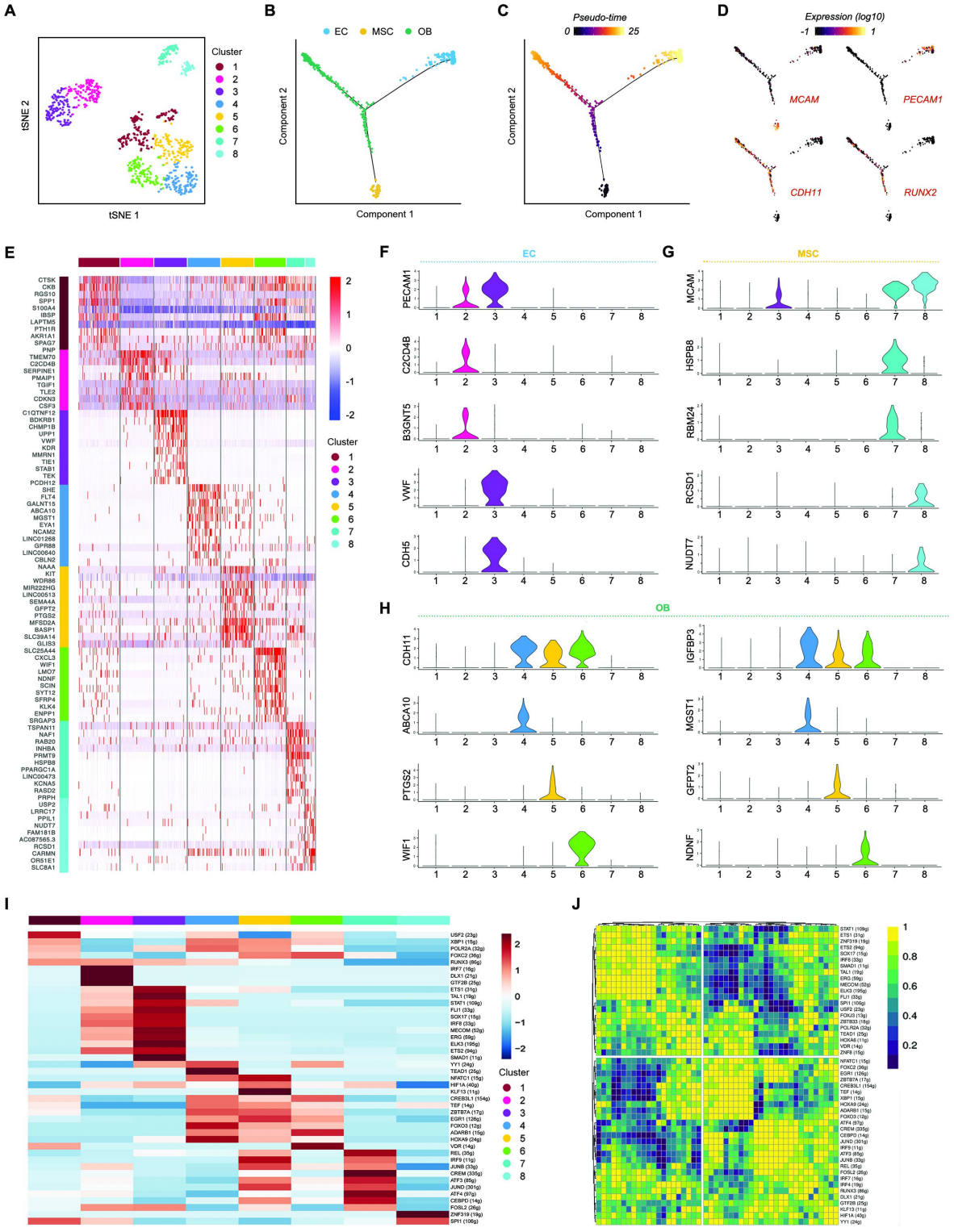

Figure2. Identification of bone related cell populations in human OA subchondral bone

(A) t-SNE plots of bone associated cells coloured by cluster. (B–D) Pseudotime trajectory plot showing differentiated cell types (endothelial cells [ECs], mesenchymal stem cells, and

593 osteoblasts [OBs]) at the end of the branches. Dots along the trajectory lines represent the
594 status of the cells transitioning toward differentiated cell types. (E) Heatmap revealing the
595 scaled expression of differentially expressed genes (DEGs) for each cluster defined in (A).
596 (F–H) Violin plots showing expression levels of indicated markers for eight clusters. (I–J)
597 Single-cell regulatory network inference and clustering analysis showing distinct regulons in
598 eight clusters. The heatmap shows only the regulons with significant differences.

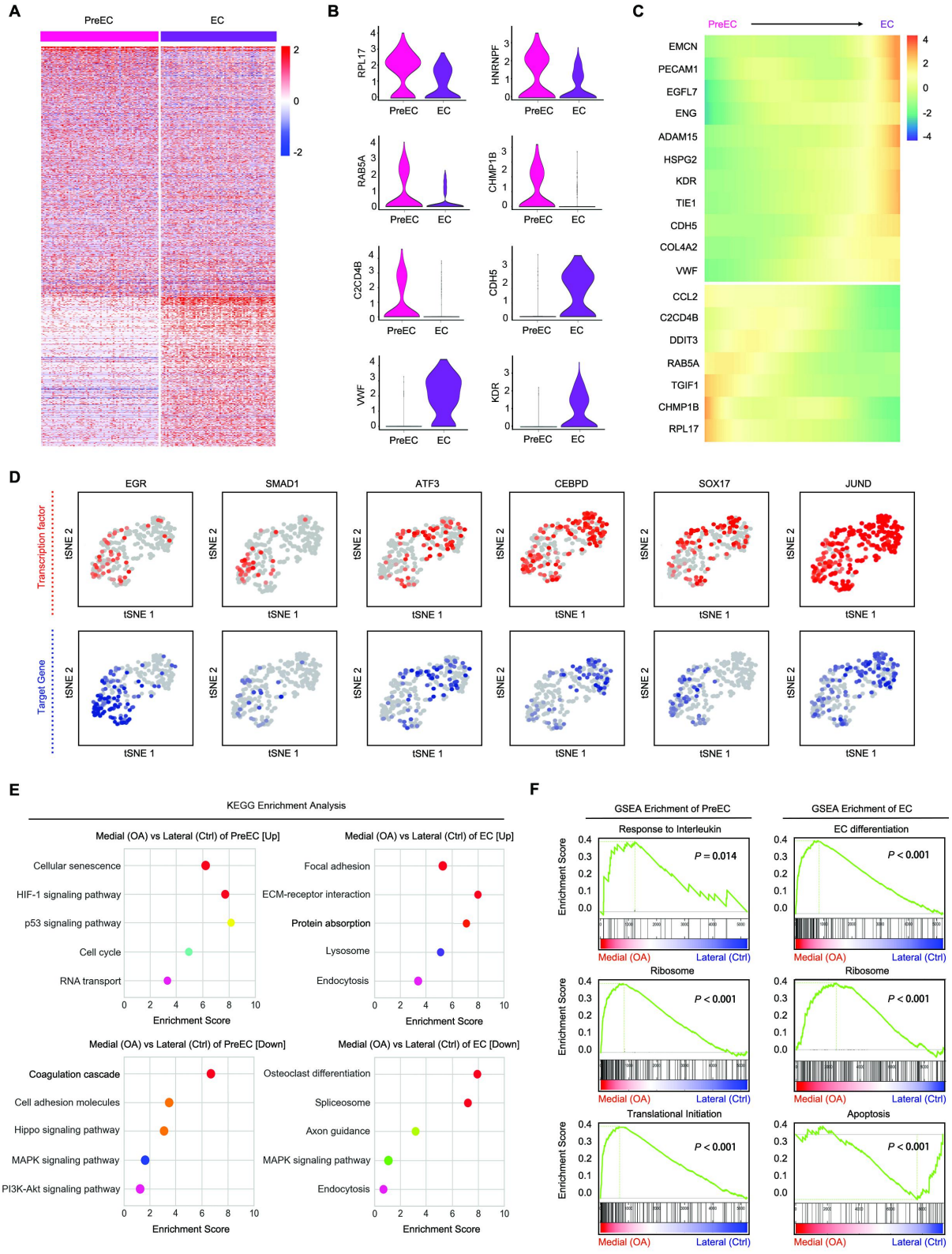

Figure3. Identification of precursor ECs (pre-ECs) and ECs

(A) Heatmap of DEGs between different ECs. (B) Violin plots showing the expression levels of

602 the specific representative genes marking pre-ECs and ECs. (C) Heatmap showing
603 upregulation or downregulation of vascular markers, exosomes, and ribosomal markers in
604 the differentiation process. (D) tSNE plots of the expression levels of transcription factors
605 (TFs; up) and area under the curve scores (down). (E) Kyoto Encyclopaedia of Genes and
606 Genomes pathway enrichment between the OA and Ctrl groups in pre-ECs and ECs. (F) Gene
607 Set Enrichment Analysis (GSEA) pathway enrichment between the OA and Ctrl groups in
608 pre-ECs and ECs.

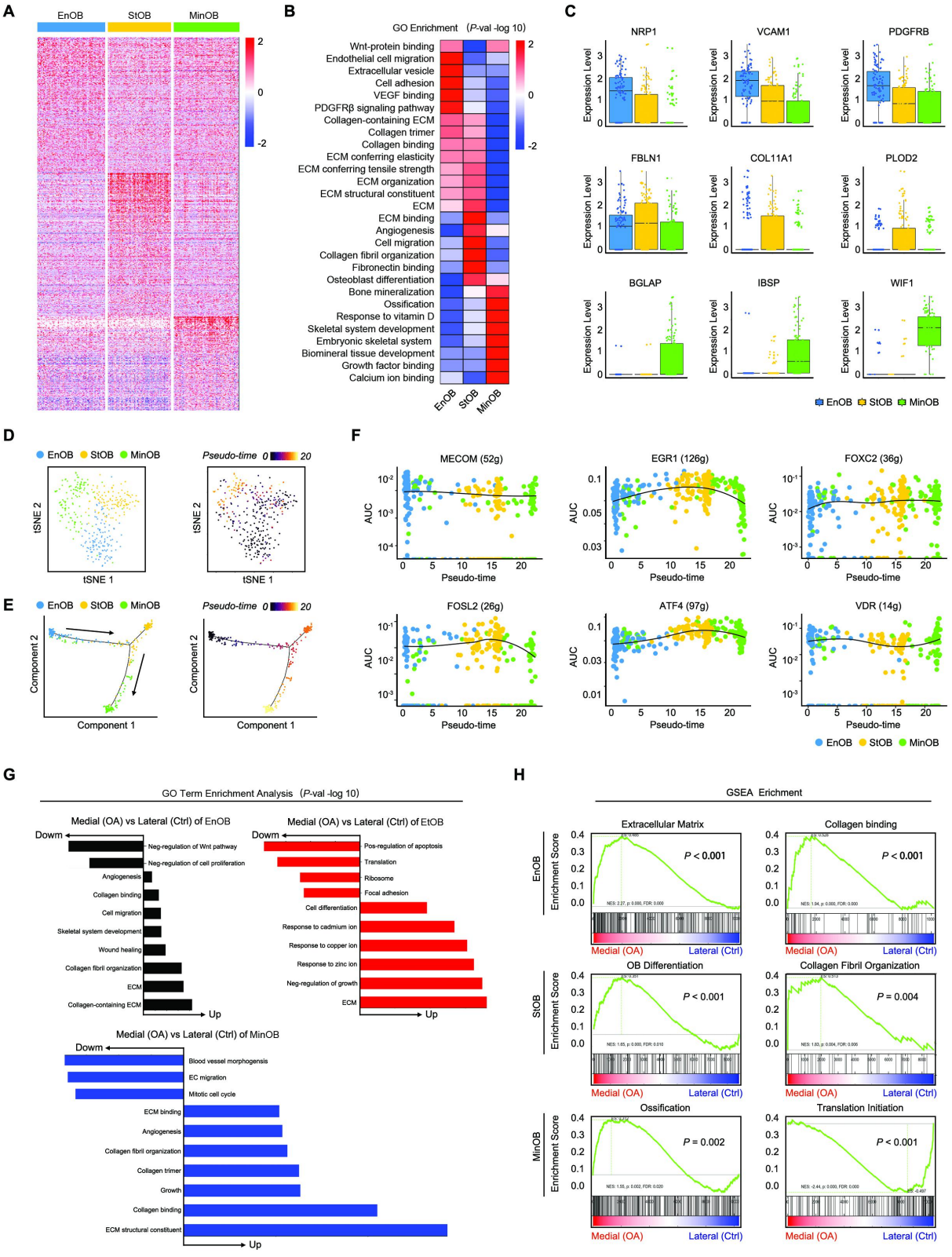

Figure4. Determining the relationships among endothelial OBs (EnOBs), stromal OBs (StOBs), and mineralised OBs (MinOBs)

612 (A) Heatmap showing Z score scaled expression levels of DEGs for EnOB, StOB, and MinOB
613 populations. (B) Heatmap showing the differences in enriched Gene Ontology (GO) functions
614 of upregulated genes in different OB subsets. (C) Boxplots showing the expression levels of
615 representative candidate marker genes specifically expressed in different subsets.
616 (D,E) Monocle pseudospace trajectory revealing the progression of OB lineage in
617 subchondral bone coloured according to cluster. Monocle pseudotime trajectory revealing
618 the progression of EnOBs, StOBs, and MinOBs. (F) Pseudotemporal expression dynamics of
619 TFs in EnOBs, StOBs, and MinOBs. All single cells in the EnOB, StOB, and MinOB cell lineage
620 are ordered based on pseudotime. (G) GO functions enrichment analysis of OA vs. Ctrl
621 upregulated genes in EnOBs, StOBs, and MinOBs. (H) GSEA showing enrichment of pathways
622 between the OA and Ctrl groups in EnOBs, StOBs, and MinOBs.

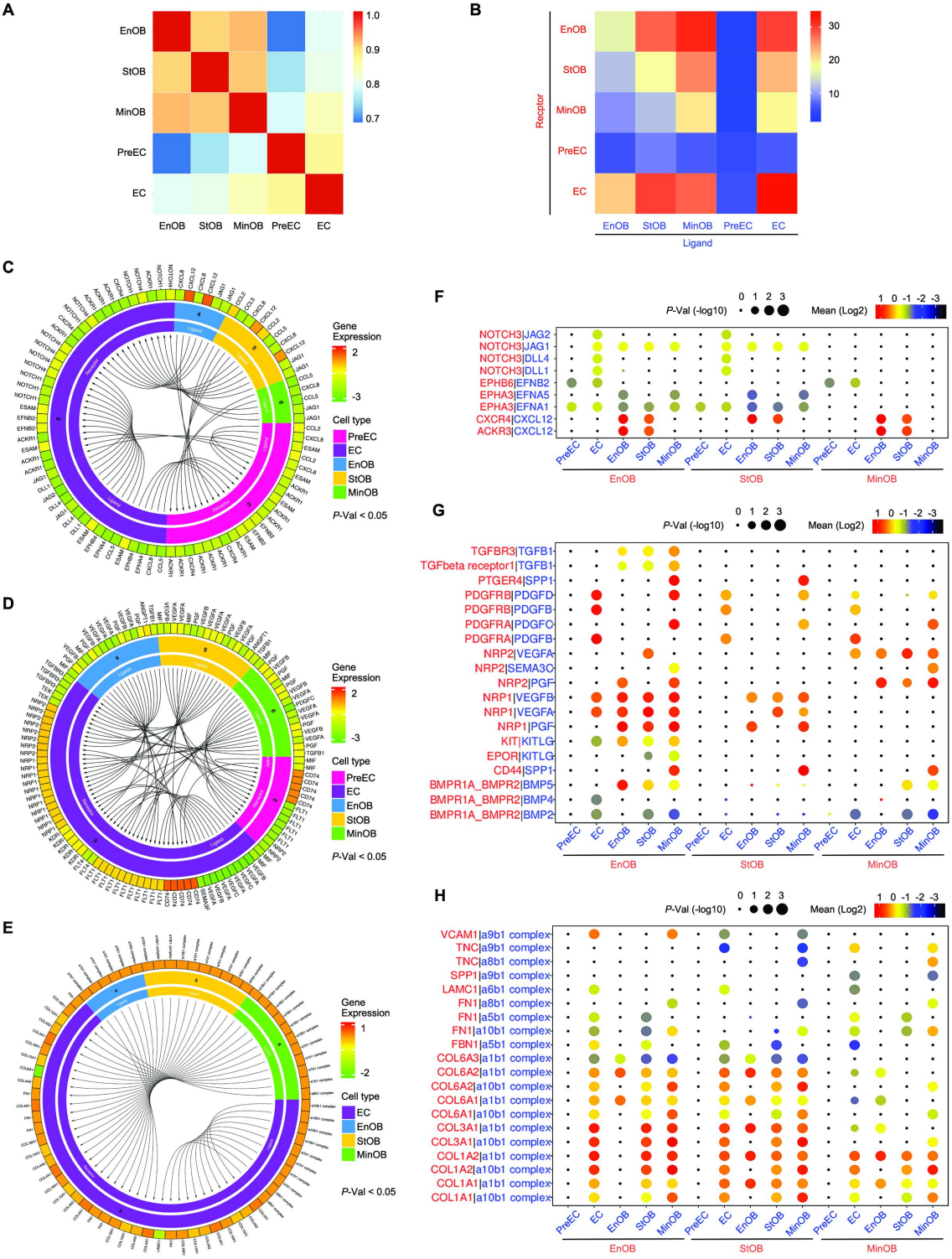

Figure 5. Vascular EC and OB subtype interaction

(A) Pearson correlation analysis of two clusters of ECs subsets and three clusters of OBs. (B) CellPhoneDB analysis showing the number of ligand-receptor interactions between EC and

627 OB subpopulations. Circos plots showing ligand-receptor pairs of cytokines (C), growth
628 factors (D), and integrin (E) between EC subpopulations. Bubble plots showing
629 ligand-receptor pairs of cytokines (F) , growth factors (G), and integrin (H) between OB
630 subpopulations.

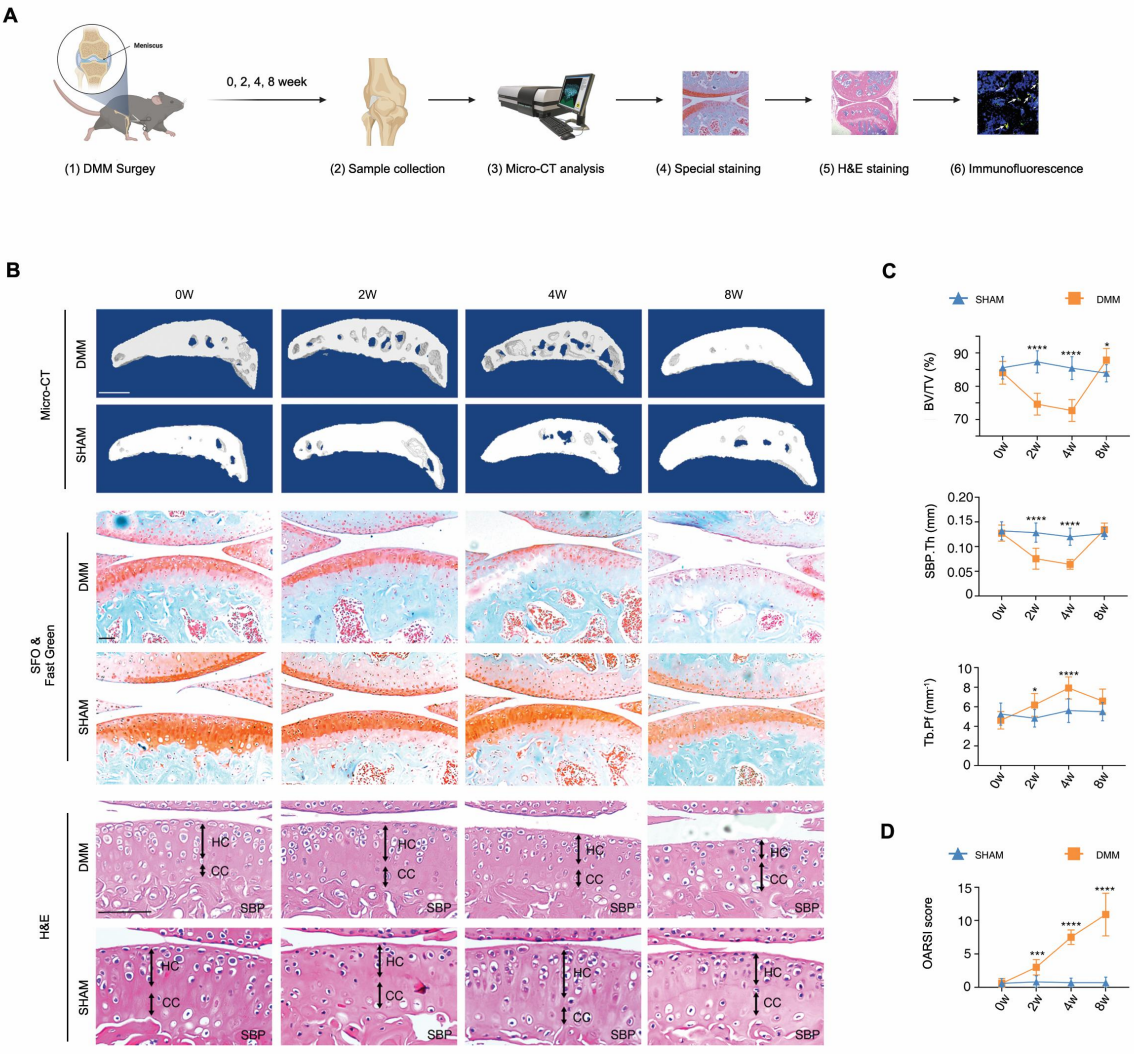

631

632 **Figure 6. Pathological identification of DMM mice model.**

633 (A) Schematic illustration of the experimental process. (B) Top row, representative
634 3-dimension image of subchondral bone from tibial medial plateau at 0, 2, 4, and 8 weeks

635 after sham or DMM surgery. Middle rows, safranin O and fast green stain of tibial medial
636 plateau at the same checkpoint. Bottom rows, H&E staining of knee joint, cartilage and
637 subchondral bone. HC: hyaline cartilage; CC: calcified cartilage; SBP: subchondral bone plate.
638 (C) Quantitative analysis of bone volume tissue/total tissue volume (BV/TV), subchondral
639 bone plate thickness (SBP. Th) and trabecular bone pattern factor (Tb.Pf) in medial plateau
640 calculated from micro-CT results. (D) Osteoarthritis Research Society International scores
641 after DMM operation are shown bottom right. n=10 in each group. Scale bar, 100 μm.
642 *p<0.05, **p<0.01, ***p<0.001, ****p<0.0001. Statistical significance was shown by
643 Two-way ANOVA. Data was presented as the mean±SD.

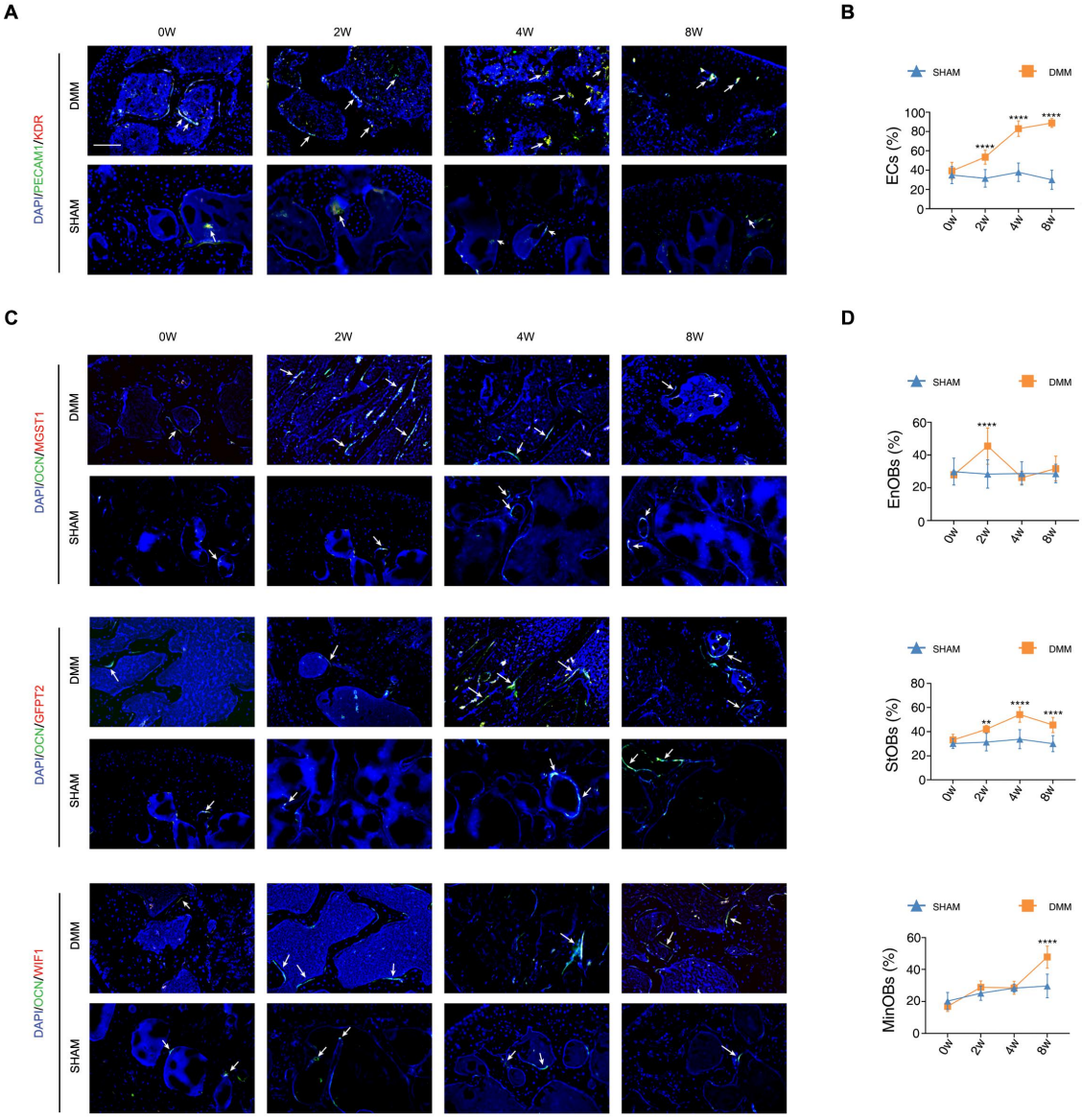

644

645 **Figure 7. Pathological identification of EC and OB subpopulations.**

646 (A) Immunofluorescence staining of PECAM1, KDR, white arrow shows co-positive area of

647 corresponding markers. (B) Percentage of PECAM1+KDR+ ECs in total PECAM1+ cells. (C)

648 Immunofluorescence staining of OCN, MGST1, GFPT2 and WIF1, white arrow shows

649 co-positive area of corresponding markers. (D) Percentage of MGST1+ EnOBs, GFPT2+ StOBs

650 and WIF1+ MinOBs in OCN+ cells, n=9 in each group. Scale bar, 100 μm. *p<0.05, **p<0.01,

651 ***p<0.001, ****p<0.0001. Statistical significance was shown by Two-way ANOVA. Data was

652 presented as the mean±SD.